LA-UR-95- 1820

CONF-9408182--5

TITLE: MULTI-SATELLITE CHARACTERIZATION OF THE LARGE ENERGETIC ELECTRON FLUX INCREASE AT L=4-7, IN THE FIVE-DAY PERIOD FOLLOWING THE MARCH 24, 1991, SOLAR ENERGETIC PARTICLE EVENT

AUTHOR(S): John C. Ingraham
Thomas E. Cayton
Richard D. Belian
Roderick A. Christensen
Fred Guyker
Michael M. Meier
Geoffrey D. Reeves

SUBMITTED TO: Proceedings of the Taos Workshop
August 14-19, 1994
Taos, NM

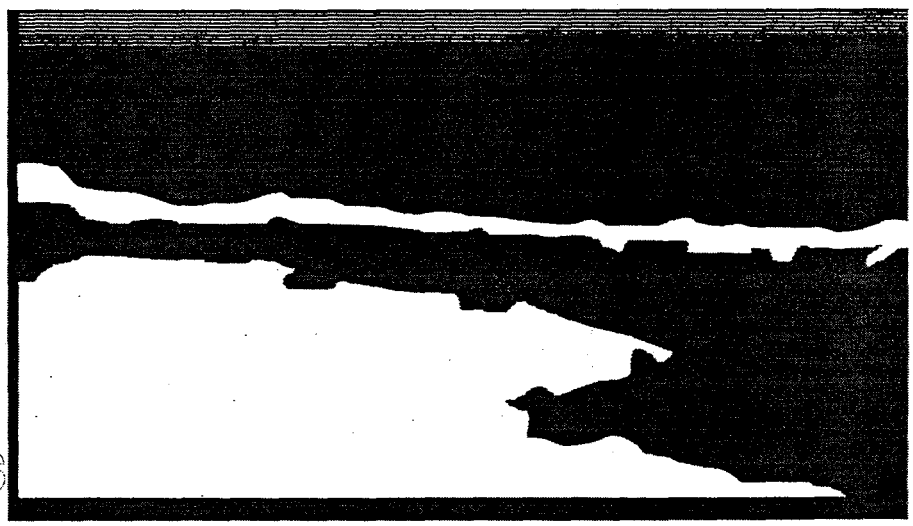

Los Alamos
NATIONAL LABORATORY

Form No. 836 R5
ST 2629 10/91

Multi-Satellite Characterization of the Large Energetic Electron Flux Increase at L=4-7, in the Five-Day Period Following the March 24, 1991, Solar Energetic Particle Event

J. C. INGRAHAM, T. E. CAYTON, R. D. BELIAN, R. A. CHRISTENSEN, F. GUYKER, M. M. MEIER, AND G. D. REEVES

NIS Division, Los Alamos National Laboratory, Los Alamos, NM

D. H. BRAUTIGAM AND M. S. GUSSENHOVEN

Phillips Laboratory, GPSP, Hanscom AFB, MA

R. M. ROBINSON

Lockheed Palo Alto Research Laboratory, Palo Alto, CA

Following the giant magnetic storm that started on March 24, 1991, and the immediately-preceding solar energetic particle (SEP) event, a dramatic increase in the flux of energetic electrons was observed to occur on several satellites (using Los Alamos instruments aboard two geosynchronous satellites and two GPS satellites, plus energetic electron data from the CRRES satellite) sampling the L=4-7 region of the magnetosphere. We find that: this flux buildup at the larger L-values (L=6-7) first appears near the magnetic equator and subsequently spreads to higher magnetic latitudes; the flux buildup near the magnetic equator peaks first at the higher L before it peaks at the lower L; analysis of the angular distribution of energetic electrons at geosynchronous orbit shows that the flux buildup begins first with the buildup of energetic electrons (>300 keV) moving perpendicular to the magnetic field.

INTRODUCTION

The purpose of this paper is to briefly summarize measurements of the several-day relativistic electron flux buildup following the March 24, 1991, magnetic storm, based on data from five satellites: two at geosynchronous orbit, two at Global Positioning System (GPS) orbit, and CRRES. (This magnetic storm, and the solar energetic particle event that preceded it, will henceforth be referred to as "the SEP".) Details of this work will be presented elsewhere [Ingraham, et al., 1995]. The multi-satellite data provide a more complete picture of the temporal and spatial behavior of the event, with regard to density, energy distribution, and pitch angle distribution, which will aid in the further development of model mechanisms in the future.

The practical importance of identifying and understanding the production mechanism for these relativistic electrons arises because they penetrate the outer skin of satellites causing radiation damage, electronic upsets, and component damage through deep dielectric charging [e. g., Baker et al., 1987; Violet and Frederickson, 1993].

SATELLITE ORBITS, INSTRUMENTATION AND DATA DESCRIPTION

Electron and proton data from several instruments (SOPA, ESP, and PSA) aboard two geosynchronous satellites, 1989-046 and 1990-095, are being used in this study, but in this paper our results, which are corroborated by the other instruments aboard both geosynchronous satellites, will be restricted to Synchronous Orbit Particle Analyzer (SOPA) data from satellite 1989-046. The 24-hour period geosynchronuous orbit is circular of radius 6.6 Earth radii (R_E), and is located in the equatorial plane. The SOPA [Belian et al., 1992] consists of three telescopes of full acceptance angle 11° oriented at angles of 30, 90, and 120 degrees relative to the Earth-directed spin axis of the satellite. It has nine differential-energy electron channels that detect electron energies from 50 keV to 1.6 MeV, an integral electron channel for energies greater than 1.6 MeV, and twelve differential-energy proton channels that detect proton energies from 50 keV to 50 MeV.

Data from electron and proton dosimeters aboard two GPS Navstar satellites, NS-10 and NS-18, are used. The dosimeter, BDD-I [Cayton et al., 1992; Drake et al., 1993], on NS-10 consists of three channels sensitive to electrons with energies greater than 0.5, 1.0, and 2.0 MeV and to protons with energies greater than 6, 10, and 15 MeV. The dosimeter, BDD-II [Feldman et al., 1985], on NS-18 consists of seven electron channels spanning 0.2 to 5.9 MeV and four proton channels spanning 9 to 50 MeV energies. Most of the GPS results presented here are based on the BDD-I data. The GPS orbits are circular of radius $4.2R_E$ and are half-synchronous, i. e., have a 12-hour orbital period. The NS-10 and NS-18 orbital planes are inclined at 63° and 55°, respectively, to the equatorial plane. Thus the BDD instruments each sample the center of the outer radiation belt, as well as open field lines toward the

poles, four times per day. The BDD dosimeters average the particle flux coming from the 2π-steradians solid angle centered on the Earth.

The primary data used from CRRES (Combined Release and Radiation Effects Satellite) comes from the CRRES Space Radiation Dosimeter [Gussenhoven et al., 1992] lowest energy channel, Dome 1, which detects electrons of energy greater than 2.0 MeV incident over a 2π steradian solid angle of acceptance [Auchampaugh and Cayton, 1993]. The Dosimeter data is spin-averaged and therefore represents an average of particle flux from all directions. Data has also been used from the Spectrometer for Electrons and Protons, S-E-P [Nightingale et al., 1992], to provide an independent confirmation of the BDD-I flux measurements [Ingraham, et al., 1995]. The CRRES orbit is a geosynchronous-transfer type, 350 by 33600 km altitude, with an 18° inclination angle and a 10-hour orbital period.

During the several-day period following the March 24 event the CRRES orbit was in an orientation that extended toward the geomagnetic tail, such that Dome 1 sampled the region between 4 and 7 R_E during the local time range of 1900-2400. In this same time period the NS-10 orbit intersected the equatorial plane at the two (approximate) local times of 0900 and 2100, and the NS-18 orbit at 0400 and 1600. Thus, the GPS and geosynchronous data together provide a good representative set of measurements for all local times during this period. On the other hand, the CRRES instruments provide data over a fairly narrow range of local times, thus providing a monitoring of the electron flux on the nightside of the Earth.

To intercompare the data from different satellites it is also necessary to characterize the satellite locations with respect to the particle drift shells. We use the Olson-Pfitzer tilt dependent static field model [Olson and Pfitzer, 1977] to estimate the magnetic field at each satellite, B_{SAT}, and to calculate the integral second adiabatic invariant (the "bounce" invariant), I, for a particle mirroring at the satellite. An L-value [McIlwain, 1961] and magnetic latitude are then associated with each satellite location by determining the location in the Earth's (tilted) dipole magnetic field having the same values of B_{SAT} and I. Though this method suffers from the usual compromising effect of the night-day asymmetry of the magnetic field, especially outside of $R = 5R_E$, it nevertheless provides a useful ordering of the data for purposes of discussion.

RESULTS

Electron Flux Buildup at Geosynchronous Orbit

The energetic particle behavior at geosynchronous orbit during the fourteen-day window that includes the March 24, 1991 event is well-summarized by the proton and electron flux measurements of SOPA on 1989-046, as shown in Figure 1. The flux of protons of energy greater than 8 MeV (Figure 1a) begins to increase early in day 82 of 1991 (March 23) as the energetic protons from the solar energetic particle event (SEP, not to be confused with S-E-P, above) first arrive at the Earth. The proton flux increases by four orders of magnitude over the subsequent 24 hours, reaching a maximum

at the time of the arrival of the strong shock of the giant solar magnetic storm, early on day 83, and thereafter decreases back to the background level over the next six days. By contrast, the flux of relativistic electrons of energy between 1.0 and 1.6 MeV (Figure 1b), shows a dramatic increase in magnitude during the several day period following the SEP, while the energetic proton flux is decaying. Clearly there is some delayed mechanism acting to cause this later buildup of intense relativistic electron fluxes. For the purposes of this paper, the buildup of the electron flux that begins at day 85.7 will be investigated, up to day 89.2 where a sharp decrease of the flux begins. (The sharp decreases of electron flux beginning at days 85.1 and 89.2 are correlated with magnetic disturbances, which are apparent in the DST index behavior. The primary electron flux decrease at day 83.2 is also, of course, correlated with the magnetic disturbance when the strong shock compresses the magnetosphere.)

Formation of a Fourth Radiation Belt During the Electron Flux Buildup

Immediately following the SEP a third radiation belt was observed to form [Blake, et al., 1992], early in day 83. During the later period of intense electron flux buildup (of interest in this paper), between days 85.7 and 89.2, a fourth (outer) radiation belt also forms, while the inner three belts change little. This is shown in Figure 2 using the CRRES Dome 1 raw data for electrons of energy greater than 2 MeV. The four selected orbital passes of CRRES show that the belt has formed by the beginning of day 87 and persists for two days. The location of the maximum of the belt flux moves inward from about L = 5.4 to L = 4.8 during this two-day period, similar to observations reported by Frank, et al. [1964]. The selection criterion for the CRRES passes was that the satellite magnetic latitude be less than 10° during the pass, in order to minimize ambiguities that could arise from large variations of the satellite distance from the magnetic equator.

Energetic Particle Behavior at GPS Orbit (NS-10)

The highly inclined GPS orbit ($R = 4.2R_E$) samples open field lines and the center of the outer radiation belt (the third belt in Figure 2) four times per day. During the post-SEP period of energetic electron flux buildup at the belt center (beginning at day 86.0 in Figure 3), the flux of the same energy electrons on open field lines remains at, or near, background levels, indicating that the source for the energetic electrons is not located on the open field lines. This is conveniently demonstrated using the BDD-I data since the instrument regularly samples the belt center and the open field lines. Figure 3 shows for day 77 through day 90 the flux of electrons of energy greater than 2 MeV (channel E3) on open field lines and at the belt center. Also shown on the figure is the flux of protons of energy greater than 15 MeV on open field lines. The decay of the energetic proton flux on open field lines (Figure 3), and on closed field lines (Figure 1a), rules out the possibility of proton signal contamination of the electron channels during the flux buildup period. Note that the electron flux on open field lines is at, or near to, its pre-SEP background level throughout the buildup of electron flux at the belt center that

begins at day 86.0. Similar comparisons for the two lower energy electron channels, E1 and E2, lead to the same conclusion.

Magnetic Latitude Dependence of Electron Flux for L = 6-7

In this section we will be comparing the time behavior of electron fluxes measured at different magnetic latitudes on different instruments, as well as on the same instrument at different parts of the satellite orbit. Figure 4 shows that the 1.0 - 1.6 MeV omnidirectional flux buildup at geosynchronous orbit (near the magnetic equator) occurs well ahead of the same flux determined from the BDD-I (at 35° magnetic latitude) measurements, reaching its plateau at day 86.6 about a day ahead of the flux measured at BDD-I. Also shown in Figure 4 is the corresponding flux measured by BDD-II on the other GPS satellite (NS-18), which demonstrates that during the plateau period from day 87.8 to day 89.1 there are no significant local time asymmetries affecting the interpretation at the GPS orbit altitude. (Note that the BDD-II data has been normalized to the BDD-I data at day 88.7 to facilitate this comparison.)

Corroborating evidence for this delay of flux buildup with increasing magnetic latitude is given in Figure 5. Here, measurements of the flux buildup by the same instrument, Dome 1, aboard CRRES, are shown for three different ranges of magnetic latitude in the L = 6.4-6.6 range. Though the data points are sparse, owing to the dual selection process applied, the trend of an increasing delay of flux buildup with increasing magnetic latitude is evident.

With regard to the question of local time asymmetries at geosynchronous altitude affecting comparison of data from different satellites, a comparison of the geosynchronous data of Figure 4 with the low magnetic latitude (< 10°) CRRES Dome 1 data of Figure 5 shows that the two time dependences are quite similar over the whole time period from day 84 to day 90. Though the CRRES data are sparse because of the selection process (low magnetic latitude and L = 6.4-6.6), all of the data fall within the narrow range of local times of 2100-2242, whereas the geosynchronous data sample all local times every 24 hours. Thus, the good agreement between the time behavior of these two fluxes shows that local time asymmetries are not affecting our interpretations in a significant way.

Pitch Angle Electron Flux Distributions at Geosynchronous Orbit

The delay of the flux buildup at the higher magnetic latitudes could be explained if the energetic electrons were first created near the geomagnetic equator with a pancake pitch angle velocity distribution, such that mirroring initially keeps them near the equator. Pitch angle scattering by turbulent or other nonadiabatic processes would allow them subsequently to spread to higher magnetic latitudes.

To test this hypothesis we have examined the pitch angle distribution time dependence of the 1.0 - 1.6 MeV electron flux at the geosynchronous orbit of 1989-046. Techniques described in a companion paper in this publication [Christensen, et al., 1995] are used to determine the direction of the magnetic

field vector and to resolve the pitch angle distribution of the electron flux relative to this direction. Figure 6 compares the count rate evolution in the pre-SEP and post-SEP periods for 12-minute averages (70 spacecraft rotations, approximately) of the pitch angle fluxes parallel and perpendicular to the magnetic field in equal solid angles of collection. In the quiet Pre-SEP times the expected local time variation is observed, in which the flux is peaked parallel to the magnetic field ("cigar distribution") at local midnight and perpendicular to the magnetic field ("pancake distribution") at local noon with the noontime flux being larger. This effect arises through the differential action of the dayside compression and nightside stretching of the magnetosphere on the drift shells of particles having different equatorial pitch angles, combined with a radially decreasing electron flux [Roederer, 1970].

However, during the post-SEP period of rapid flux growth from day 85.6 to day 87.0 the pitch angle distribution favors the pancake distribution throughout, even at local midnight (day 86.4). This result is more clearly demonstrated in Figure 7, where Figure 7a shows a 3-day pre-SEP plot of the fractional difference between the perpendicular and parallel flux, and Figure 7b shows a 3-day post-SEP plot of the same fractional difference during a period that includes the rapid electron flux growth. A 6-hour sliding average has been applied to the data to reduce the fluctuations. The local midnight period at day 86.4 of the post-SEP period can now be seen, on average, to be nearly as pancake-like as the local noon data of the pre-SEP period. Furthermore, this tendency toward the pancake distribution is present throughout the rapid flux-growth period, but has decreased noticeably by day 87.5 when the electron flux measured at L = 6-7 and magnetic latitude 35° is approaching its plateau (Figure 4).

Returning to the 12-minute time resolution data of Figure 6, a careful examination shows that there is no time during the rapid growth phase from day 85.9 to day 87 when the flux parallel to the magnetic field exceeds the flux perpendicular to the magnetic field. There are two periods, during times of strong fluctuation at day 86.37 and day 86.46, when the two fluxes are nearly equal, but these are very brief, scarcely lasting longer than the resolution time of the measurement. Thus, the pancake-like bias of the pitch angle distribution is retained during the rapid growth phase even on a relatively short time scale.

Radial Transport on the Magnetic Equator

Figure 2 suggests some inward transport of the E > 2 MeV electrons during the formation of the fourth radiation belt. The same data, binned according to L = 4.5, 5.5 and 6.5, is plotted versus time in Figure 8. Because of the paucity of data points, owing to the highly selective binning process, the inward "motion" is apparent now only in the time of occurence of the flux maximum at the three L-values (as noted on the Figure).

SUMMARY AND DISCUSSION

The multisatellite data presented above on the buildup of the intense relativistic electron flux in the several-day period following the March 24, 1991, giant magnetic storm has provided a more complete picture of the essential features of such a buildup.

1. On open field lines the flux of electrons of energy greater than 1 MeV remains near quiet-time pre-storm levels throughout the buildup of the same energy group of electrons on closed field lines.

This indicates that for this particular event the immediate source of the these energetic electrons is not external to the magnetosphere, such as would be the case for Solar or Jovian electrons [Baker et al., 1986].

2. In the L = 6-7 region ,

a. the flux buildup first appears at low magnetic latitudes near the geomagnetic equator and subsequently spreads to higher magnetic latitudes. The typical delay for the appearance of a given flux feature at magnetic latitude of 35°, relative to the geomagnetic equator, is about one day.

b. analysis of the evolution of the pitch angle distribution at the geomagnetic equator shows that during the rapid growth of the electron flux the distribution is concentrated preferentially perpendicular to the magnetic field in a pancake distribution at all local times, even on a relatively short time scale. As would be expected, toward the end of the growth phase at the magnetic equator, when the flux is beginning to build up at 35° magnetic latitude, the pitch angle distribution has become significantly less pancake-like and is approaching the distribution characteristic of more quiet times before the storm.

These results together lead to the conclusion that in the L = 6-7 region the electron energization mechanism acts preferentially near the geomagnetic equator to increase the electron energy perpendicular to the magnetic field, and that pitch angle scattering subsequently allows the energized electrons to spread to higher magnetic latitudes.

3. In the L = 4-5 region the flux buildup is qualitatively similar to that at L = 6-7, appearing first near the magnetic equator and then spreading to higher magnetic latitudes, but is less well defined. For example, no delay is seen at L = 4-5 between the 0-10° and 10-20° magnetic latitudes at L = 4-5 (not shown in figures).

This result is consistent with the interpretation that the dominant transport is radially inward with the pitch angle scattering that happens between L = 6.5 and 4.5 acting to reduce the magnetic latitude contrast at L = 4.5. However, this conclusion is somewhat weakened because here we are constrained to compare measurements of the same energy range of electrons at the two L-values; what should be compared, of course, is the corresponding phase space volumes of electrons at the two L-values.

4. A radially inward transport of electrons (E > 2 MeV) as the fourth belt forms is suggested by Figure 2. This picture is supported by Figure 8, which shows that the peak of the flux occurs first at L = 6.5, and then in turn at L = 5.5 and 4.5 [see also, Frank, et al., 1964].

It is also significant that the measured "plateau flux" at L = 4.5, as shown in Figure 8 for electrons of greater than 2 MeV energy, is only about a factor of 3.6 greater than this flux measured by the same

instrument at L = 6.5. A rough estimate of the change of the flux measured in this channel if a 90-degree pitch angle distribution is transported from L = 6.5 to L = 4.5 while conserving the first adiabatic invariant, μ, predicts an increase between a factor of 40 and 180. This implies that μ is not conserved in such a case, which is consistent with the hypothesis that pitch angle scattering is occurring as the electrons are transported inward.

CONCLUSIONS

These multisatellite results indicate quite clearly that some alternative magnetospheric electron energization mechanism should be sought to explain the electron flux buildup following the March 24, 1991, giant magnetic storm, other than the recirculation process within the magnetosphere [Nishida, 1976; Baker et al., 1989; Fujimoto and Nishida, 1990] or a direct source of Solar or Jovian energetic electrons [Baker et al., 1979, 1986]. In order to be a viable candidate for electron energization for this particular event, a mechanism must preferentially act to increase the electron energy perpendicular to the magnetic field in a region near to the magnetic equator in the outer magnetosphere, while not drawing upon energetic electrons on open field lines as a direct source of energization.

Acknowledgements. The authors would like to thank Karl Pfitzer of McDonnell Douglas Space Systems Company for providing us with a copy of the computer code for the tilt-dependent magnetic field model[Olson and Pfitzer, 1977]. This work was supported under the auspices of the United States Department of Energy.

REFERENCES

Auchampaugh, G., and T. Cayton, CRRES dosimeter simulations, *LA-12511-MS*, 51 pp., Los Alamos National Laboratory, Los Alamos, New Mexico, 1993.

Baker, D. N., P. R. Higbie, R. D. Belian, and E. W. Hones, Jr., Do Jovian electrons influence the terrestrial outer radiation zone?, *Geophys. Res. Lett.*, *6*, 531, 1979.

Baker, D. N., J. B. Blake, R. W. Klebesadel, and P. R. Higbie, Highly relativistic electrons in the Earth's outer magnetosphere: 1. Lifetimes and temporal history 1979-1984, *J. Geophys. Res.*, *91*, 4265, 1986.

Baker, D. N., R. D. Belian, P. R. Higbie, R. W. Klebesadel, and J. B. Blake, Hostile energetic particle radiation environments in Earth's outer magnetosphere, *J. of Electrostatics, 20*, 3, 1987.

Baker, D. N., J. B. Blake, L. B. Callis, R. D. Belian, and T. E. Cayton, *Geophys. Res. Lett.*, *16*, 559, 1989.

Belian, R. D., G. R. Gisler, T. Cayton, and R. Christensen, High-Z energetic particles at geosynchronous orbit during the great solar proton event series of October 1989, *J. Geophys. Res.*, *97*, 16897, 1992.

Blake, J. B., W. A. Kolasinski, R. W. Fillius, and E. G. Mullen, Injection of electrons and protons with energies of tens of MeV into L < 3 on 24 March 1991, *Geophys. Res. Lett.*, *19*, 821, 1992.

Cayton, T. E., P. R. Higbie, D. M. Drake, R. C. Reedy, D. K. McDaniels, R. D. Belian, S. A. Walker, L. K. Cope, E. Noveroske, and C. L. Baca, BDD-I: An electron and proton dosimeter on the Global Positioning System-Final Report, *LA-12275* , 71 pp., Los Alamos National Laboratory, Los Alamos, New Mexico, 1992.

Christensen, R. A., T. E. Cayton, R. D. Belian, and M. M. Meier, Pitch angle distributions of relativistic electrons at geostationary orbit, this conference proceedings.
Drake, D. M., T. E. Cayton, P. R. Higbie, D. K. McDaniels, R. C. Reedy, R. D. Belian, S. A. Walker, L. K. Cope, E. Noveroske and C. L. Baca, Experimental evaluation of the BDD-I dosimeter for the Global Positioning System, *Nucl. Instr. Methods, A333,* 571, 1993.
Feldman, W., W. Aiello, D. Drake, and M. Herrin, The BDD II: An improved electron dosimeter for the Global Positioning System, *LA-10453-MS*, 18 pp., Los Alamos National Laboratory, Los Alamos, New Mexico, 1985.
Fujimoto, M., and A. Nishida, Energization and anisotropization of energetic electrons in the Earth's radiation belt by the recirculation process, *J. Geophys. Res., 95*, 4265, 1990.
Frank, L. A., J. A. Van Allen, and H. K. Hills, A study of charged particles in the Earth's outer radiation zone with Explorer 14, *J. Geophys. Res., 69*, 2171, 1964.
Gussenhoven, E. G. Mullen, M. Sperry, and K. J. Kerns, The effect of the March 1991 storm on accumulated dose for selected satellite orbits: CRRES dose models, *IEEE Trans. on Nucl. Science, 39*, 1765, 1992.
Ingraham, J. C., T. E. Cayton, R. D. Belian, R. A. Christensen, F. Guyker, M. M. Meier, G. D. Reeves, D. H. Brautigam, M. S. Gussenhoven, and R. M. Robinson, *The large energetic electron flux increase at L=4-7, in the five-day period following the March 24, 1991, giant magnetic storm: multi-satellite measurements*, submitted to J. Geophys. Res., 1995.
McIlwain, C. E., Coordinates for mapping the distribution of magnetically trapped particles, *J. Geophys. Res., 66*, 3681, 1961.
Nightingale, R. W., R. R. Vondrak, E. E. Gaines, W. L. Imhof, R. M. Robinson, S. J. Battel, D. A. Simpson, and J. B. Reagan, CRRES spectrometer for electrons and protons, *J. of Spacecraft and Rockets, 29,* 614, 1992.
Nishida, A., Outward diffusion of energetic particles from the Jovian radiation belt, *J. Geophys. Res., 81*, 1771, 1976.
Olson, W. P., and K. A. Pfitzer, Magnetospheric magnetic field modeling, annual scientific report, Air Force Off. of Sci. Res., contract F44620-75-C-0033, 96 pp., McDonnell Douglas Astronaut. Co., Huntington Beach, Calif., 1977.
Roederer, J. G., *Dynamics of Geomagnetically Trapped Radiation*, Springer-Verlag, New York, 1970.
Violet, M. D., and A. R. Frederickson, Spacecraft anomalies on the CRRES satellite correlated with the environment and insulator samples, *IEEE Trans. on Nucl. Science, 40*, 1512, 1993.

J. C. Ingraham, T. E. Cayton, R. D. Belian, R. A. Christensen, F. Guyker, M. M. Meier, and G. D. Reeves , MS D436, NIS-2, Los Alamos National Laboratory, Los Alamos, NM87545
D. H. Brautigam and M. S. Gussenhoven
Phillips Laboratory, GPSP, Hanscom AFB, MA 01731
R. M. Robinson
Lockheed Palo Alto Research Laboratory, Palo Alto, CA 94304

INGRAHAM ET AL.: ENERGETIC ELECTRON FLUX INCREASE AT L = 4 - 7

Fig. 1. Particle flux behavior (5-minute averaged) at geosynchronous orbit before, during and after the SEP that ended early on March 24, 1991 (Day 83): (a), protons of energy greater than 8 MeV, and (b), electrons of energy between 1 and 1.6 MeV.

Fig. 2 Growth of fourth radiation belt during the rapid relativistic electron flux growth period, as measured with the CRRES Dosimeter (1.8-minute averaged data) for four passes through the radiation

belts. The times, in Decimal Days, when the satellite is at L = 6.7 (vertical dashed line) are indicated for each of the passes on the figure.

Fig. 3 Evolution from before to after the SEP of energetic electron fluxes on open field lines and at the belt center, and of the energetic proton flux on open field lines at GPS orbit (BDD-I on NS-10).

Fig. 4 Comparison of the energetic 1-1.6 MeV electron flux time behavior after the SEP, as measured at geosynchronous orbit (SOPA, 1989-046) and at GPS orbit (NS10 and NS18) for times when the three satellites were between L = 6 and L = 7.

Fig. 5 Electron flux buildup (E > 2 MeV), as measured by Dome 1 on CRRES for three magnetic latitude ranges at L = 6.5, showing the larger delay of the buildup at the larger magnetic latitudes.

Fig. 6 Time behavior of the parallel and perpendicular components of the pitch angle distribution (12-minute averaged) of 1 - 1.6 MeV electrons at geosynchronous orbit (SOPA, 1989-046), from before to after the SEP.

Fig. 7 Fractional difference of perpendicular minus parallel energetic (1 - 1.6 MeV) electron pitch angle flux components (6-hour averaged) at geosynchronous orbit for three-day periods, (a), before the SEP, and (b), during the electron flux growth after the SEP.

Fig. 8 Energetic electron flux buildup (E > 2 MeV) for three L-values and magnetic latitude < 10°, as measured by Dome 1 on CRRES. The arrows indicate the times for each L-value when the flux is a maximum.

Fig. 1a

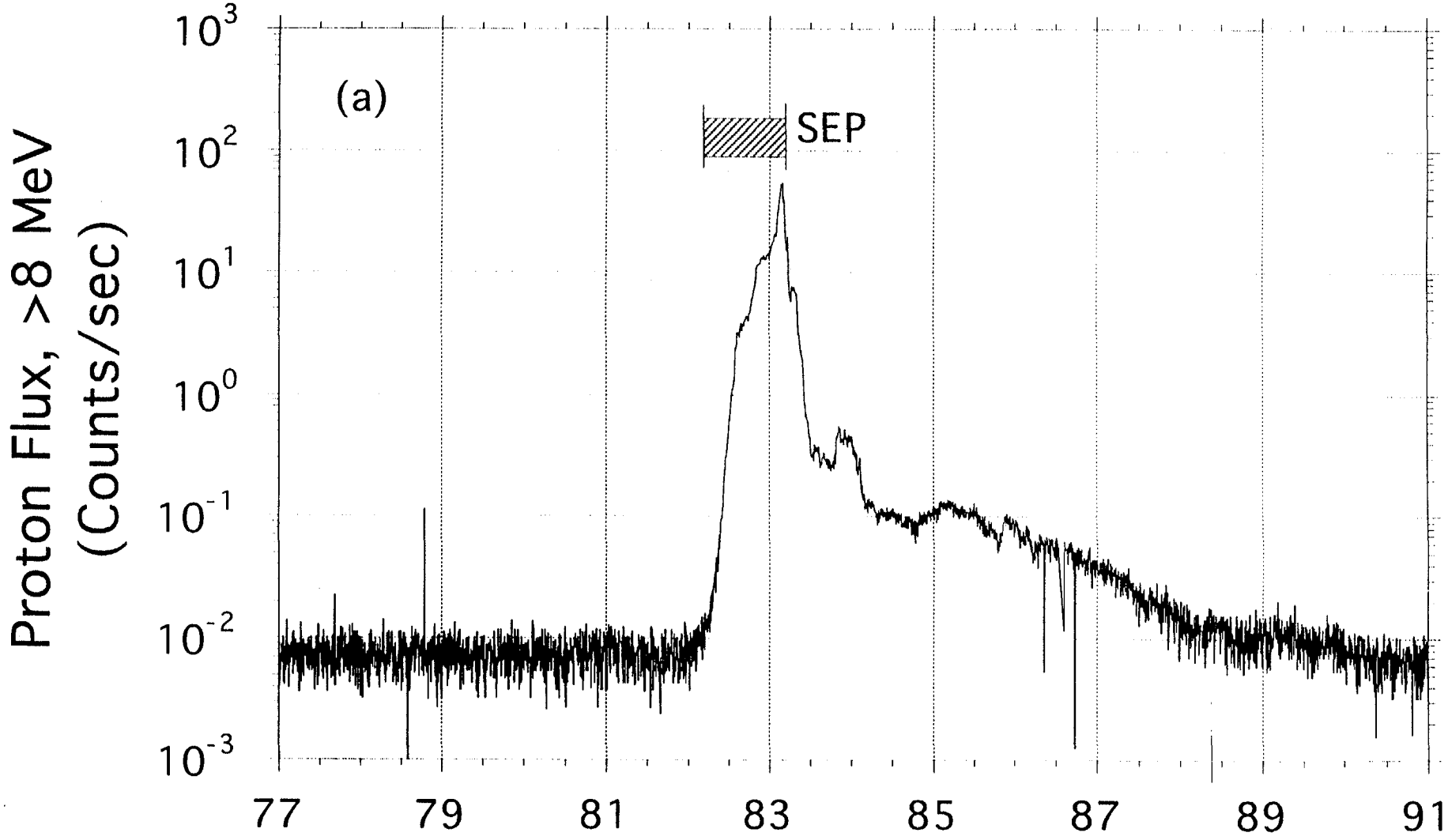
(a)
SEP
Proton Flux, >8 MeV
(Counts/sec)
10^3
10^2
10^1
10^0
10^{-1}
10^{-2}
10^{-3}
77
79
81
83
85
87
89
91

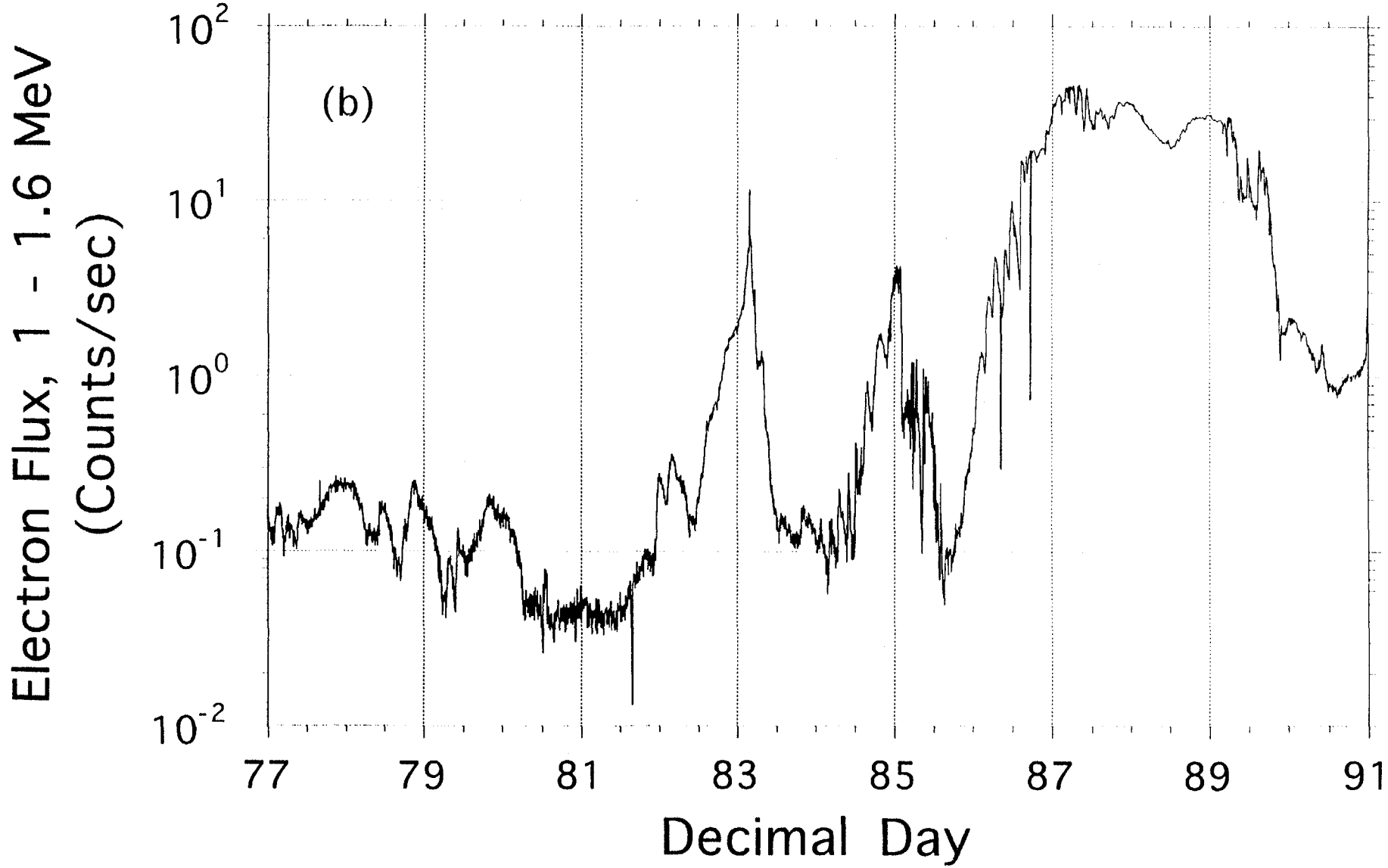
(b)
Electron Flux, 1 - 1.6 MeV
(Counts/sec)
10^2
10^1
10^0
10^{-1}
10^{-2}
77
79
81
83
85
87
89
91
Decimal Day

Fig. 2

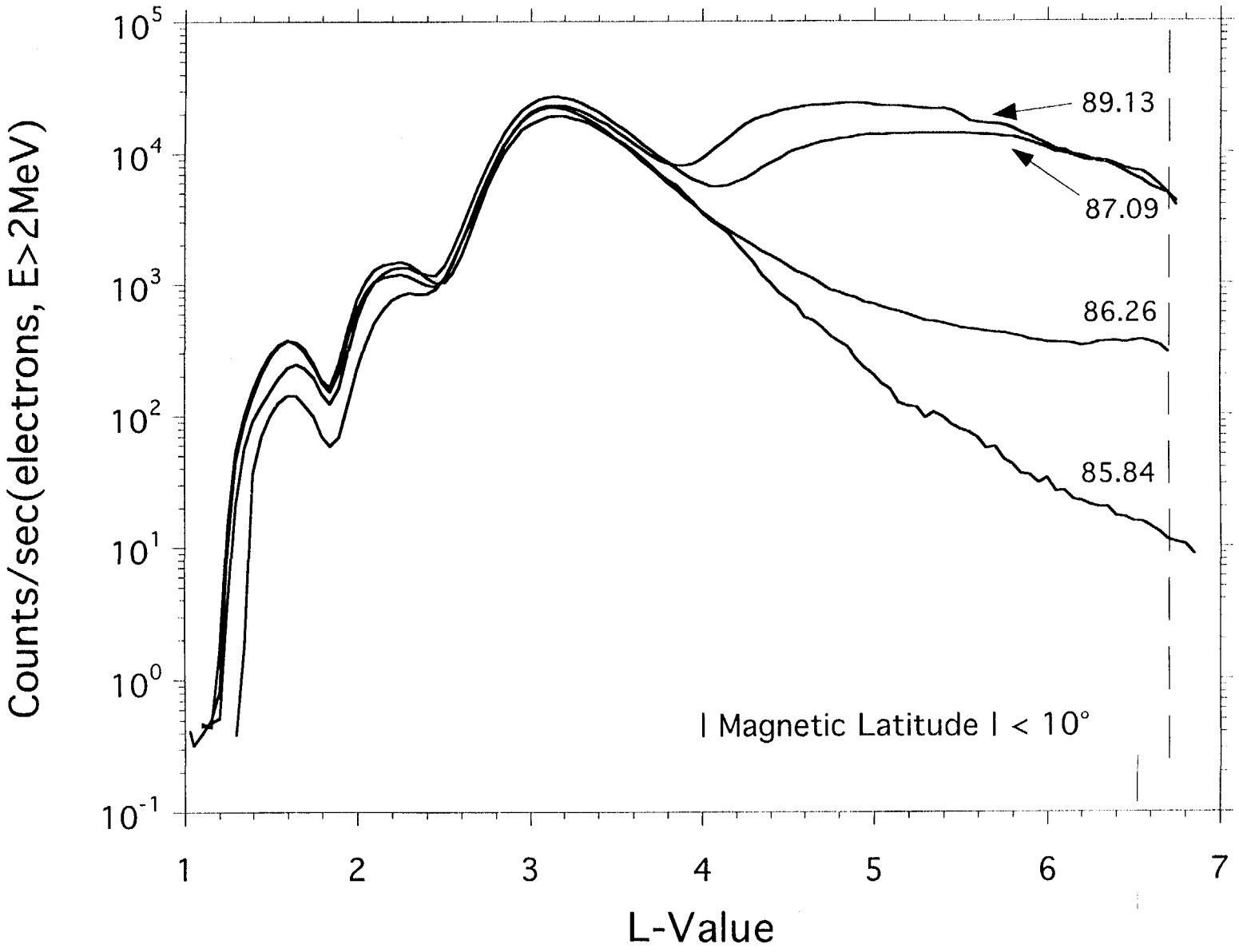
Counts/sec(electrons, E>2MeV)
10^5
10^4
10^3
10^2
10^1
10^0
10^{-1}
89.13
87.09
86.26
85.84
| Magnetic Latitude | < 10°
1
2
3
4
5
6
7
L-Value

Fig. 3

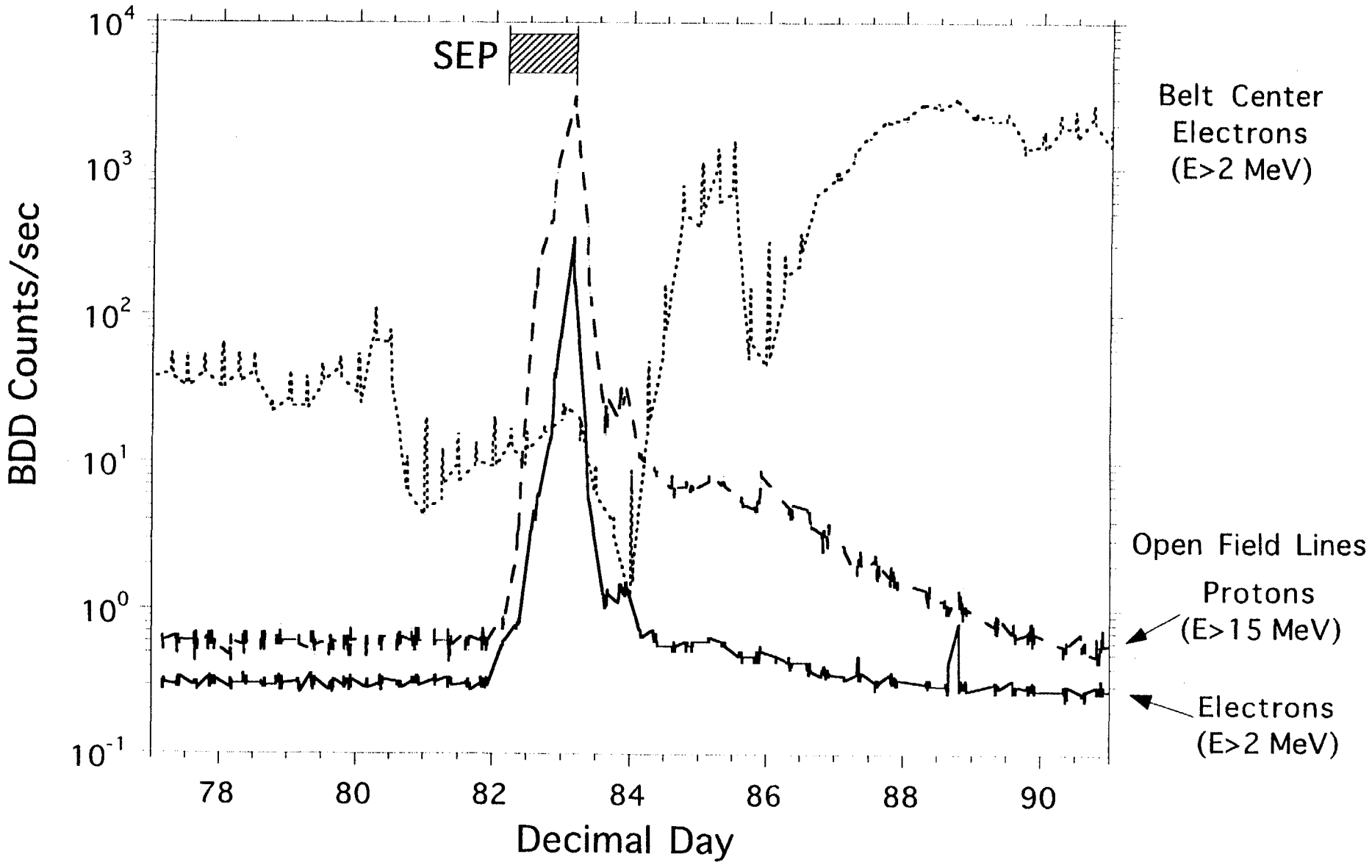
SEP
Belt Center
Electrons
(E>2 MeV)
Open Field Lines
Protons
(E>15 MeV)
Electrons
(E>2 MeV)
BDD Counts/sec
10^4
10^3
10^2
10^1
10^0
10^{-1}
78
80
82
84
86
88
90
Decimal Day

Fig. 4

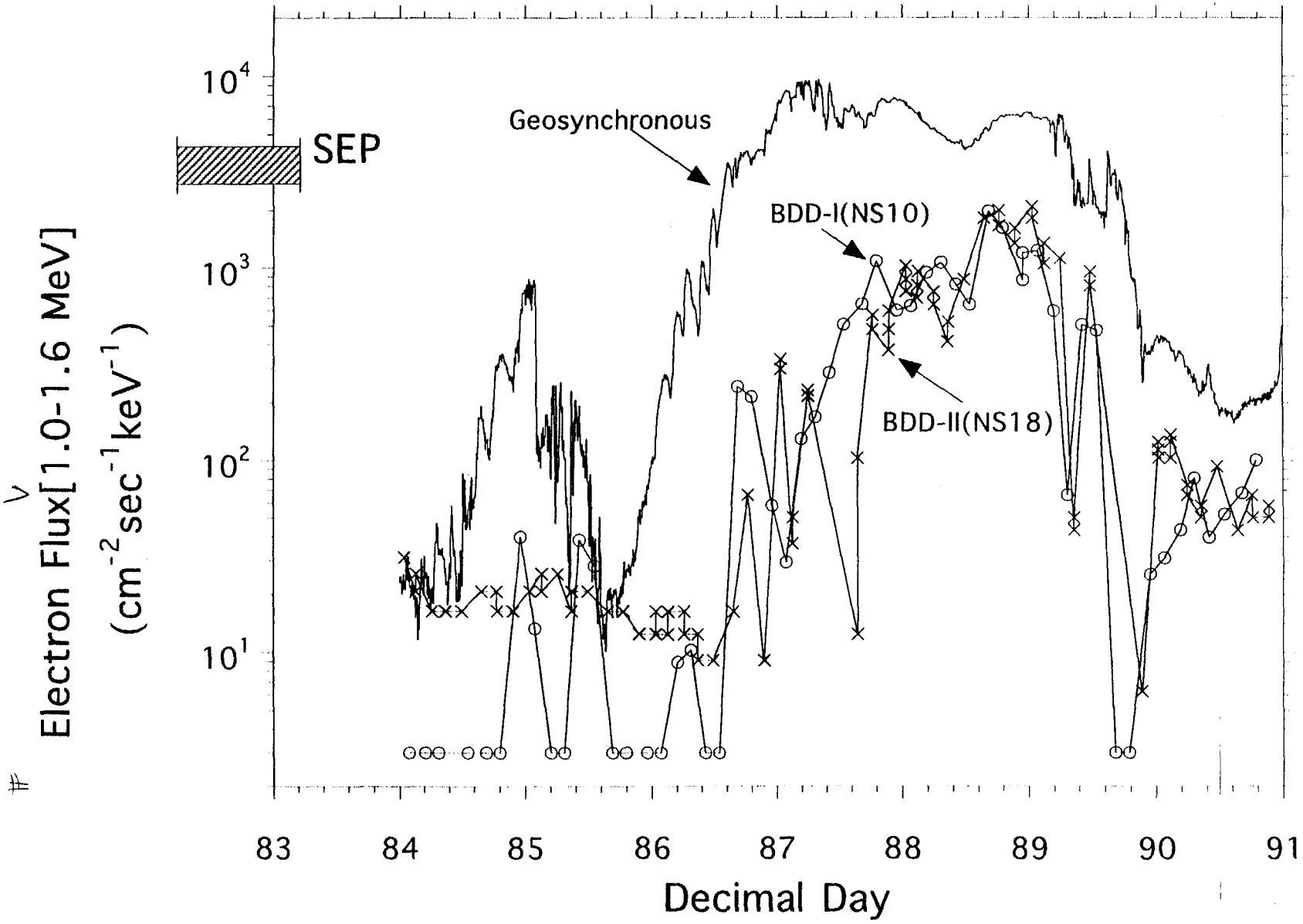
SEP
Geosynchronous
BDD-I(NS10)
BDD-II(NS18)
Electron Flux[1.0-1.6 MeV]
(cm^{-2}sec^{-1}keV^{-1})
10^4
10^3
10^2
10^1
83
84
85
86
87
88
89
90
91
Decimal Day

Fig. 5

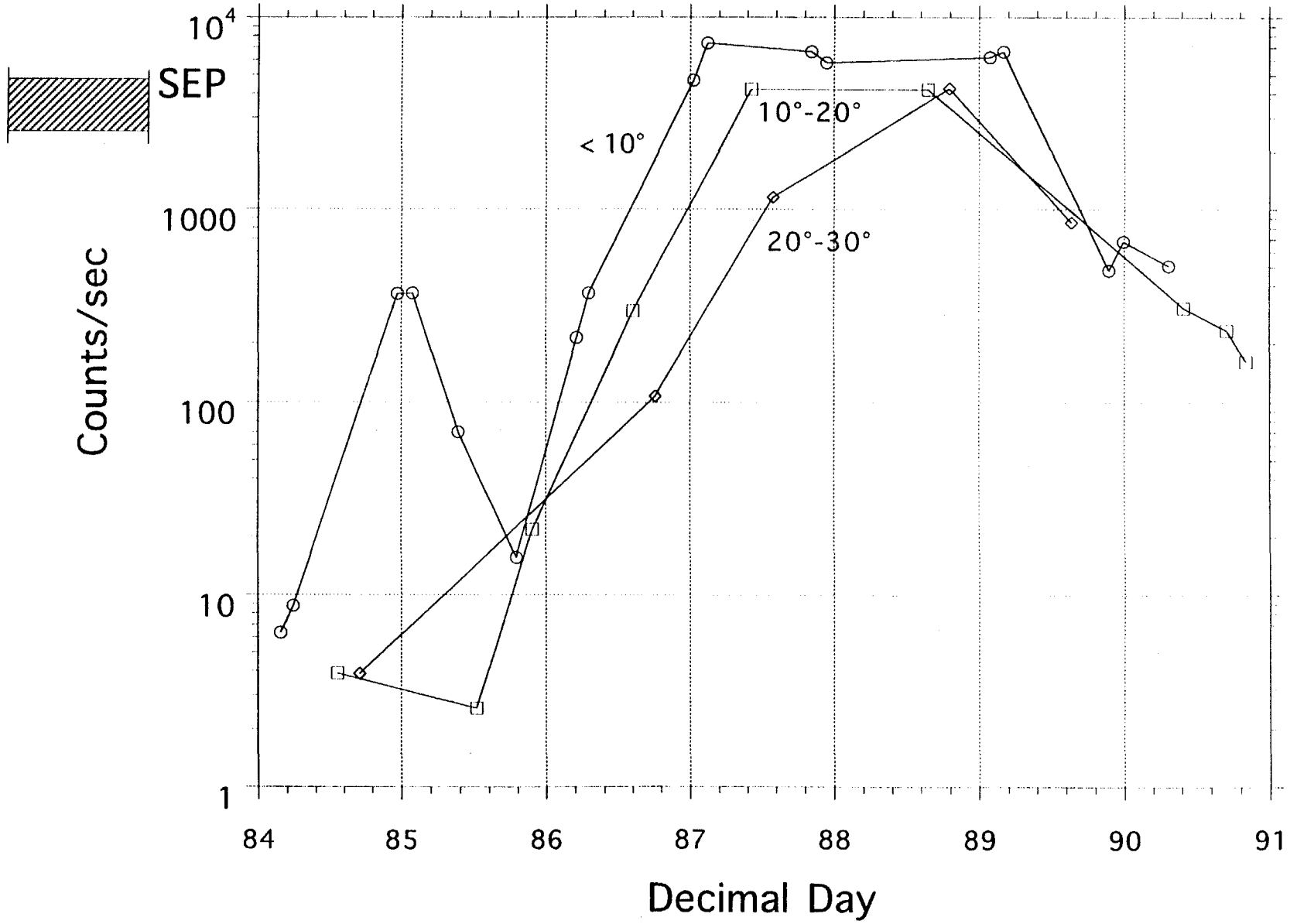
SEP
10^4
1000
100
10
1
Counts/sec
< 10°
10°-20°
20°-30°
84
85
86
87
88
89
90
91
Decimal Day

Fig. 6

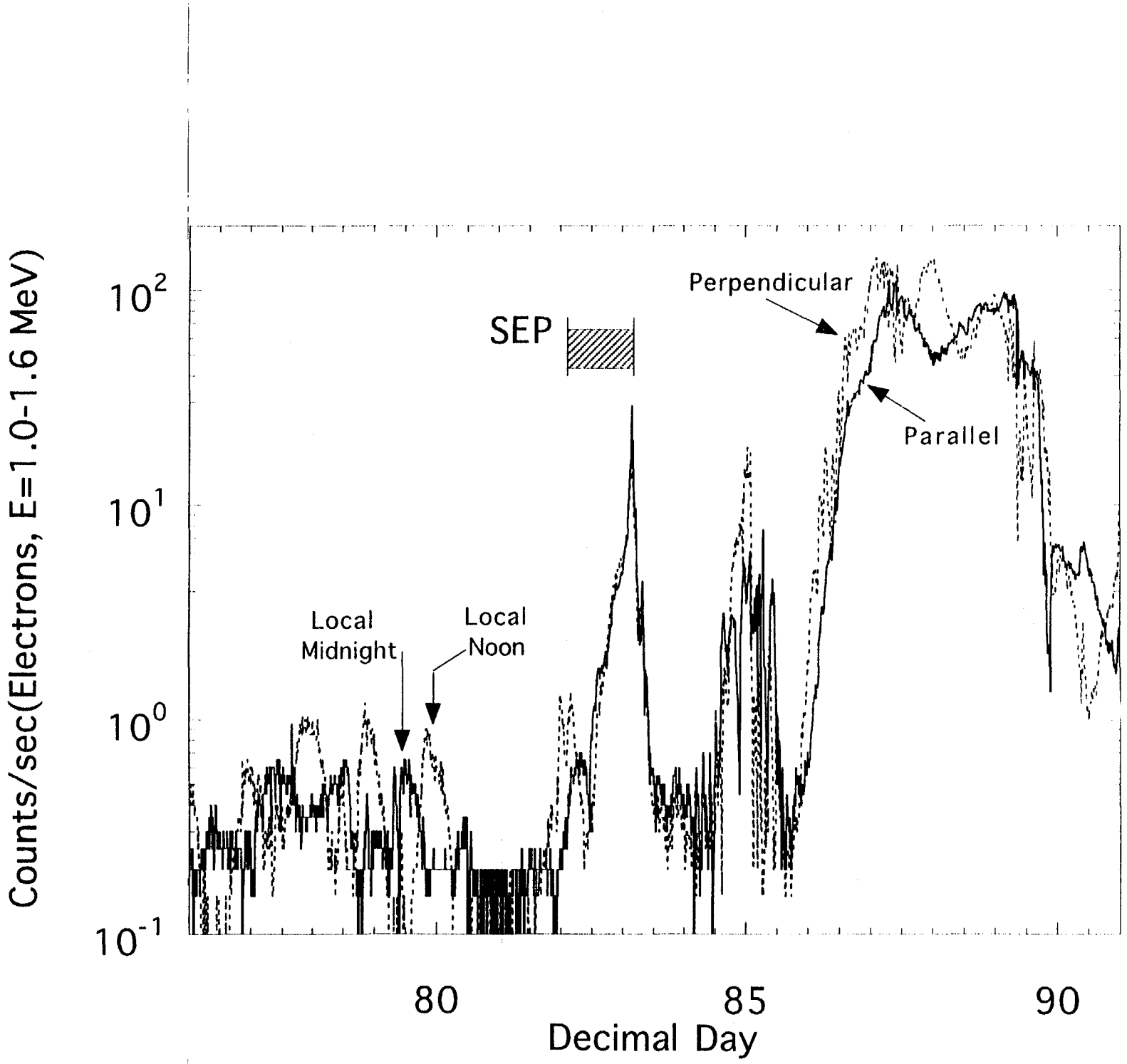
Counts/sec(Electrons, E=1.0-1.6 MeV)
10^2
10^1
10^0
10^{-1}
SEP
Perpendicular
Parallel
Local Midnight
Local Noon
80
85
90
Decimal Day

Fig. 7a

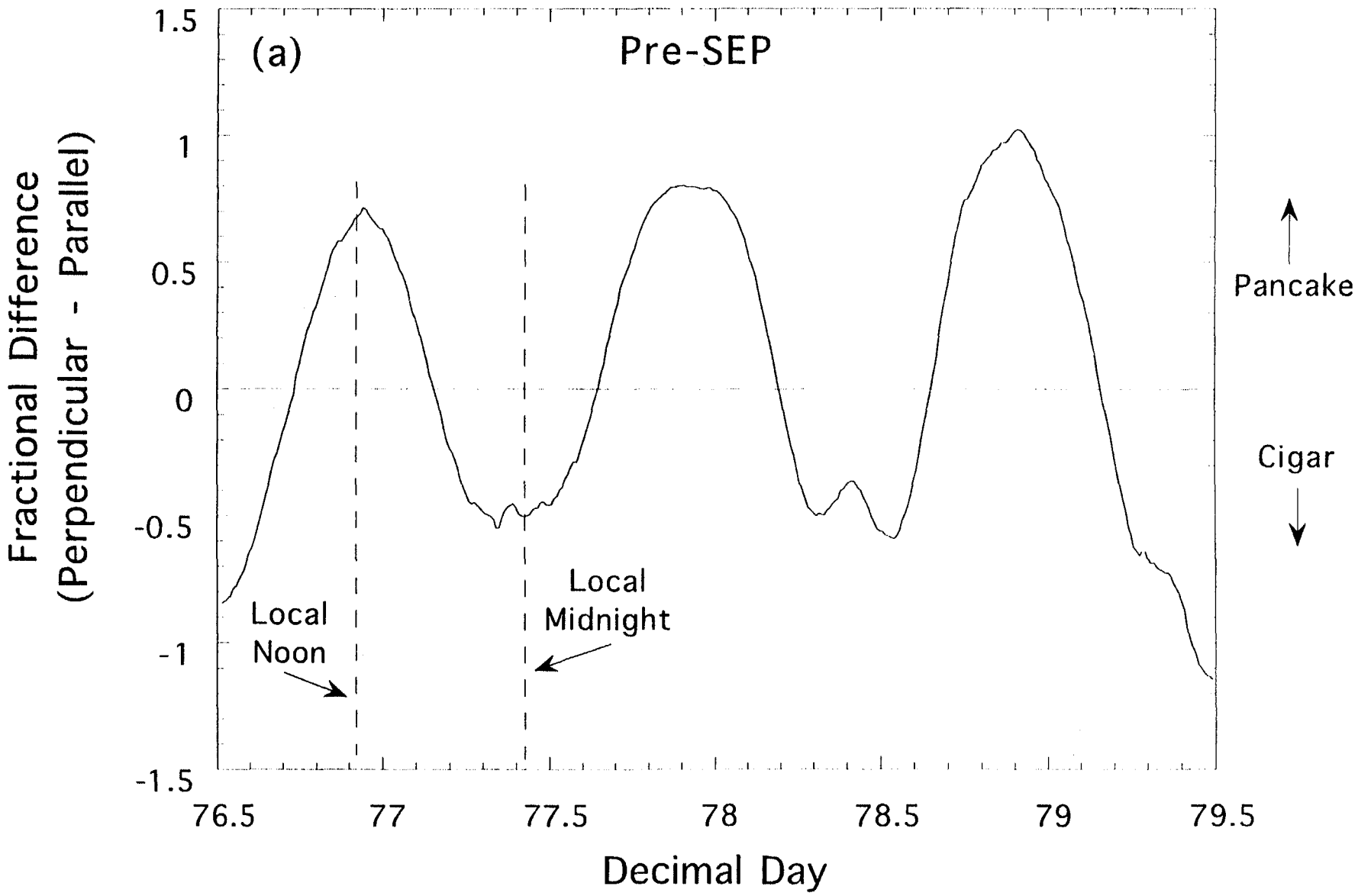
(a)
Pre-SEP
Fractional Difference
(Perpendicular - Parallel)
1.5
1
0.5
0
-0.5
-1
-1.5
Local
Noon
Local
Midnight
Pancake
Cigar
76.5
77
77.5
78
78.5
79
79.5
Decimal Day

Fig. 7b

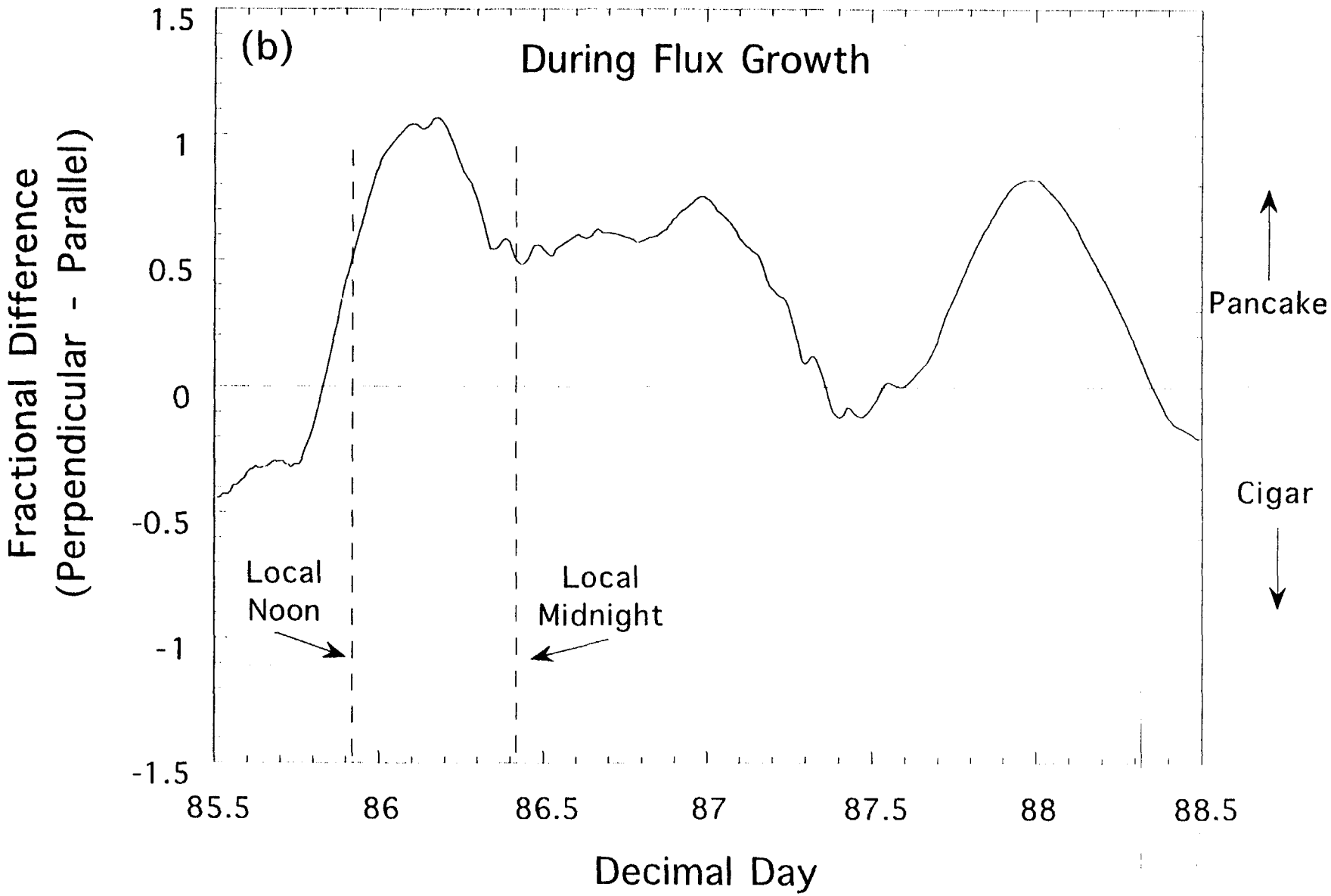
(b)
During Flux Growth
Fractional Difference
(Perpendicular - Parallel)
1.5
1
0.5
0
-0.5
-1
-1.5
Local
Noon
Local
Midnight
Pancake
Cigar
85.5
86
86.5
87
87.5
88
88.5
Decimal Day

fig. 8

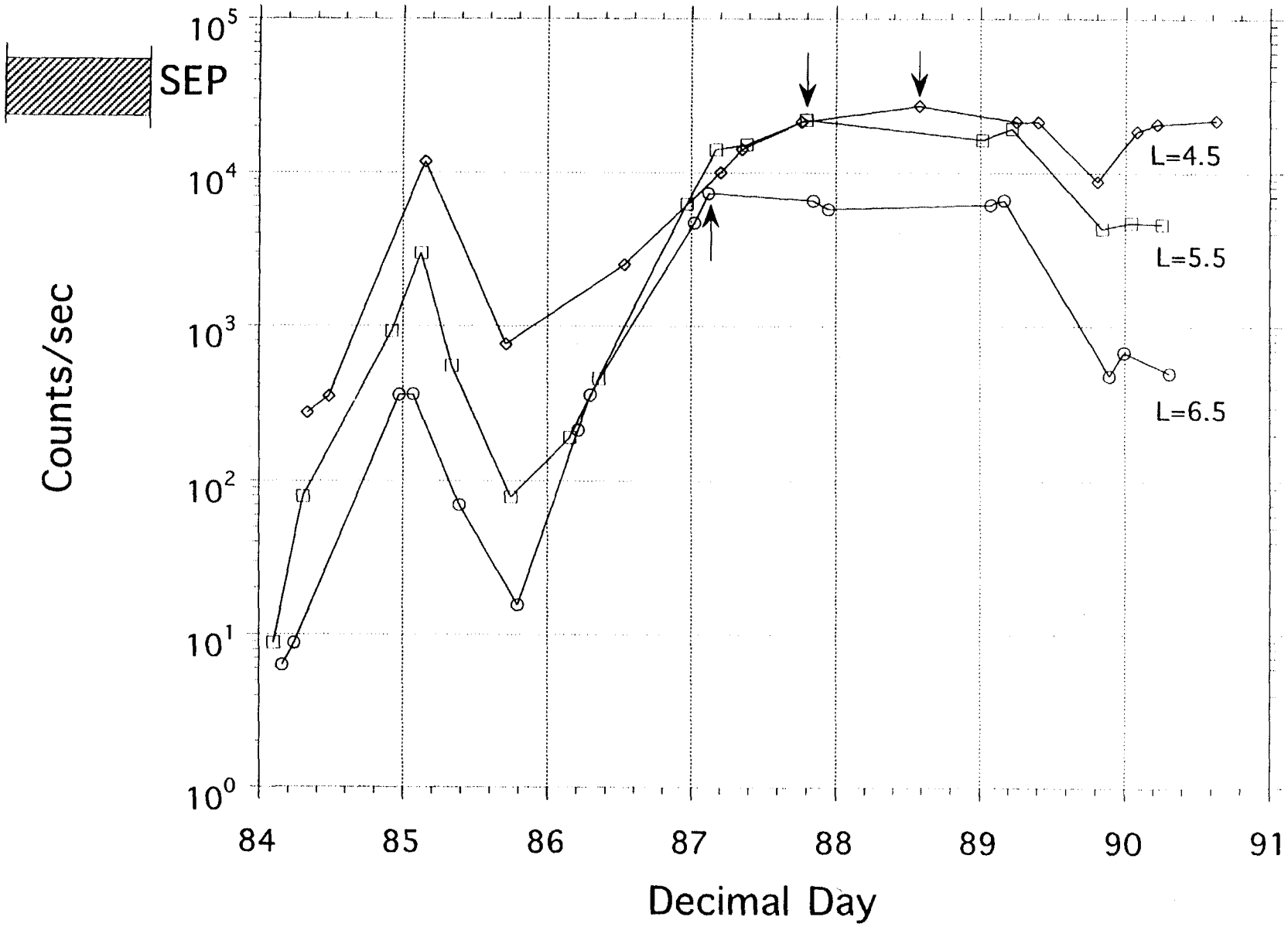
SEP
Counts/sec
10^5
10^4
10^3
10^2
10^1
10^0
L=4.5
L=5.5
L=6.5
84
85
86
87
88
89
90
91
Decimal Day